

Review

A Review of Numerical Research on the Pressure Swing Adsorption Process

Runye Zhang ¹, Yuanhui Shen ¹, Zhongli Tang ¹, Wenbin Li ² and Donghui Zhang ^{1,*}

¹ The Research Center of Chemical Engineering, School of Chemical Engineering and Technology, Tianjin University, Tianjin 300072, China; zhangrunye@tju.edu.cn (R.Z.); shenyh@tju.edu.cn (Y.S.); zltang@tju.edu.cn (Z.T.)

² Collaborative Innovation Center of Chemical Science and Engineering (Tianjin), School of Chemical Engineering and Technology, Tianjin University, Tianjin 300072, China; richard@tju.edu.cn

* Correspondence: donghuizhang@tju.edu.cn

Abstract: The pressure swing adsorption (PSA) process has been considered a promising method for gas separation and purification. However, experimental methods are time-consuming, and it is difficult to obtain the detailed changes in variables in the PSA process. This review focuses on the numerical research developed to realize the modelling, optimization and control of the cyclic PSA process. A complete one-dimensional mathematical model, including adsorption bed, auxiliary devices, boundary conditions and performance indicators, is summarized as a general modelling approach. Key simplified assumptions and special treatments for energy balance are discussed for model reliability. Numerical optimization models and control strategies are reviewed for the PSA process as well. Relevant attention is given to the combination of deep-learning technology with artificial-intelligence-based optimization algorithms and advanced control strategies. Challenges to further improvements in the adsorbent database establishment, multiscale computational mass transfer model, large-scale PSA facility design, numerical computations and algorithm robustness are identified.

Keywords: PSA; numerical modelling; optimization; control



Citation: Zhang, R.; Shen, Y.; Tang, Z.; Li, W.; Zhang, D. A Review of Numerical Research on the Pressure Swing Adsorption Process. *Processes* **2022**, *10*, 812. <https://doi.org/10.3390/pr10050812>

Academic Editors: Simant Upreti and Federica Raganati

Received: 17 January 2022

Accepted: 17 April 2022

Published: 20 April 2022

Publisher's Note: MDPI stays neutral with regard to jurisdictional claims in published maps and institutional affiliations.



Copyright: © 2022 by the authors. Licensee MDPI, Basel, Switzerland. This article is an open access article distributed under the terms and conditions of the Creative Commons Attribution (CC BY) license (<https://creativecommons.org/licenses/by/4.0/>).

1. Introduction

Pressure swing adsorption (PSA) is a typical cyclic process, in which multiple columns are interconnected and operated according to a specified sequence to realize gas separation and purification [1]. As a commercial, robust and flexible separation unit, PSA has been widely applied in the fields of air separation, hydrogen purification, carbon dioxide capture, biogas upgrading, low-concentration syngas enrichment and so on [2–6].

According to the principle of gas separation, the adsorption and desorption behavior of adsorbate—adsorbent pairs is closely related to the separation performance. Therefore, most efforts in PSA technology have focused on the use of adsorbents with high selectivity (material science), and the design/operation of efficient processes (engineering) [7]. Fabian et al. conducted a CO₂-PSA warm gas separation technology with a ZnO sorbent for IGCC power plants, wherein the cost of electricity would reach up to 127.2 \$/MWh within one year [8]. The practical cost of hydrogen production from steam reforming with a vacuum PSA unit was around 5 EUR/kg of hydrogen as well [9]. The naturally dynamic character and complexity of the PSA process occurring there required high investment and tedious features for experimental investigations [10]. In contrast, numerical simulations are recognized as the dominant method for research and optimization work at a reduced cost [11]. The numerical modeling and simulation of the PSA process has been established in a series of mathematical models comprising mass, momentum, and energy conservation, as well as thermodynamics and kinetics [12,13], which can be described by a set of second-order partial differential and algebraic equations (PDAEs) with initial conditions and

boundary conditions. The formation of a more complete model means an increase in the number of differential equations and functional dependencies by which the model coefficients are calculated [14]. Hence, to describe different PSA processes, some variants of mathematical models needed to be taken into account, such as heat transfer between a gas and adsorbent, gas intra-diffusion transfer in an adsorbent and mass and heat transfer coefficients during sorption. Considering that the reliability of simulation results is fundamentally determined by the description and establishment of the adsorption behavior and mathematical models, it is necessary to analyze the advantages and disadvantages of model assumptions and the scope of their use in this review.

Various commercial numerical platforms have been applied for the modeling of the PSA process, such as Aspen Adsorption [15], gPROMS [16,17], MATLAB [18] and FLUENT [19]. The common approach used by the numerical calculations is the method of lines (MOL), which can discretize spatial derivatives to convert PDAEs to differential-algebraic equations (DAEs) or algebraic equations (AEs) and then solve them through different solvers. For the simulation and optimization of the PSA process with complex models and cyclic features, the solution of AEs is difficult to converge and will produce different calculation results. In addition, numerical integration of the DAEs system is complicated and time-consuming, to guarantee the performance accurately and capture the process' dynamic features simultaneously [20], especially dealing with highly nonlinear isotherms, due to numerical dispersion (smearing) and oscillation. All that has also greatly increased the difficulty of process optimization [21]. To reduce the computation amounts for simulation and optimization, researchers have proposed a variety of different surrogate models, such as the polynomial surface response model (PRSM) [22], Kriging model [23], proper orthogonal decomposition [24–26], polynomial regression model (PNR), support vector regression, and artificial neural network (ANN) model [27,28]. The surrogate model is essentially a black-box model, which is built from a known sample of input–output data points, and can be used to predict the output response at untried points/configurations [25,29]. Limited by the number of samples, the accuracy and feasibility of the surrogate model still need further verification and benchmarking studies to extend its application.

After determining the process model, it is also necessary to optimize the PSA process to find the best design parameters and operating variables to improve process efficiency. The optimization of the PSA process is a multi-objective optimization problem, which generally includes various process performance indicators, such as product purity, recovery rate, production capacity, process energy consumption, etc. For decades, various optimization strategies and algorithms have been continuously developed, which can be roughly divided into deterministic and metaheuristics algorithm. Gradient-based deterministic algorithms include sequential quadratic programming (SQP), reduced space sequential quadratic programming (rSQP), the interior point method, the efficient set method, the trust region efficient algorithm, etc. [30–32]. Novel metaheuristic and artificial-intelligence-based optimization algorithms, including the genetic algorithm (GA), particle swarm optimization (PSO), the ant colony algorithm, the annealing algorithm, etc. Among these, GA and PSO are typical metaheuristic algorithms, which have demonstrated superior performance and efficiency in multiple reports [31,33,34]. Currently, the research on PSA process optimization shows a clear trend toward a more intelligent, easier, and integrated direction. The combination of deep-learning technology with artificial-intelligence-based optimization algorithms will be new task for PSA industrial application. In addition, in actual industrial production, there are inevitably some uncertain factors that cause disturbance to the PSA process, such as feed flow, concentration and temperature deviating from the operation set, which make it take a long time to recover, resulting in suboptimal results of the entire process. Therefore, it is necessary to develop and design the control system to minimize impact and achieve stable operation. Researchers have actively explored the control system for a PSA unit, including the proportional-integral-derivative control strategy (PID) and model-predictive control strategy (MPC) [17,35].

To clarify the progress in the numerical research on PSA simulation, optimization and control, and promote the PSA technology in actual engineering applications, the paper is arranged as follows: In Section 2, some model assumptions and special treatments for energy balance are discussed, and then a complete one-dimensional mathematical model including adsorption bed, auxiliary devices, boundary conditions and performance indicators is summarized for a general PSA-process design. In Section 3, first, optimization strategies and algorithms for different process models, such as the single discrete model, fully discrete model, and surrogate model, are reviewed. Moreover, the PID controller and model predictive controller are introduced, respectively, when facing external disturbances or parameter fluctuations in the process. Finally, we summarize the whole work and point out some instructive future directions.

2. PSA Modeling

At present, the numerical simulation based on adsorption theory is a promising method for PSA-process design. It can analyze the continuous distribution of physical quantities that is difficult to obtain through experiments and explore process-design variables more quickly. The fundamental of simulation is the mathematical model; as PSA is a periodic, cyclic, and dynamic process, its mathematical models are quite complex. Li et al. [12] summarized the mathematical modeling pathway map, which comprised the correspondence between the real physical scenario and mathematical model for carbon capture by adsorption (CCA). As Figure 1 shows, a typical mathematical model for the adsorption bed contains a mass-transfer model, energy-transfer model and momentum-transfer model to describe the transfer process that occurs between gas and adsorbent. In addition to the above three models, strict adsorption-bed models also include the adsorption-kinetics model and adsorption-equilibrium model. Among them, the mass-transfer model strictly includes diffusion in the axial and radial directions, but the radial diffusion coefficient is difficult to measure and estimate. Adsorption kinetics is to study the adsorption process of external diffusion, internal diffusion and surface-adsorption behavior; the adsorption-equilibrium model describes the static-adsorption equilibrium of a single component or multicomponent on the surface of a solid adsorbent after the external diffusion and internal diffusion of gas. Different adsorption-equilibrium-isotherm models will produce different predictions, and the selection of a suitable model can help to improve the accuracy of numerical calculations. A complete process simulation also needs to consider the auxiliary module models such as tank, the valve, pump, and pipeline and performance indicators such as purity, recovery and energy consumption. Exceptionally, for a system with simple cycle schedules such as air separation, the virtual moving-bed modeling methodology, which considers only mass and energy balances and adsorption isotherms, can be employed to describe the cyclic steady state [3]. To avoid complicated numerical computations, some key assumptions frequently used will be discussed, as follows.

2.1. Adsorption-Kinetics Model

In the aspect of kinetic models, three representative adsorption-kinetic models are taken into consideration. First, a homogeneous-solid or pore-diffusion model (HSDM) has been used to describe intraparticle mass transfer [36]. This model assumes that the adsorbent is homogeneous and that the adsorption process occurs at the external surface, followed by the diffusion of the adsorbate into the interior of the adsorbent particles [37]. The mathematical expression for intraparticle diffusion is shown in Equation (1).

$$\frac{\partial q_i}{\partial t} = \frac{D_e}{r^2} \frac{\partial}{\partial r} \left(r^2 \frac{\partial q_i}{\partial r} \right) \quad (1)$$

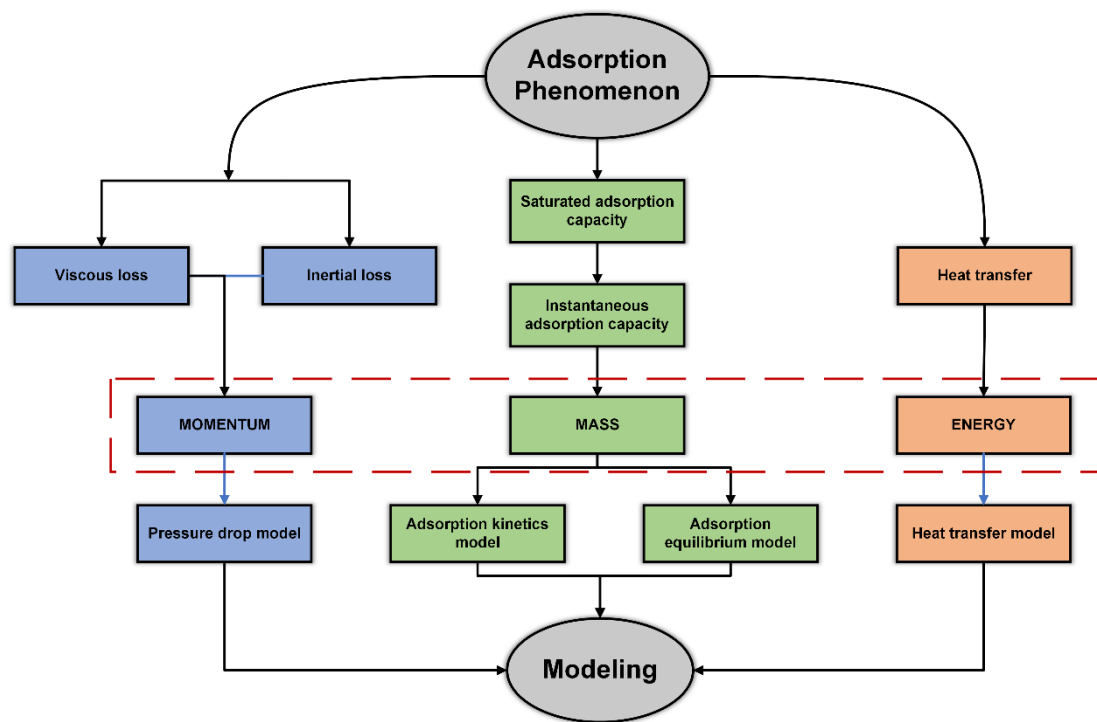


Figure 1. The CCA mathematical modeling pathway map cited from Li et al. [12]. Readapted with permission from Ref. [12]. Copyright 2018 Elsevier.

The pore-diffusion model further shows that the microstructure of particles consists of very small pores and that diffusion occurs in the internal void fraction [38]. A simplified model was proposed to calculate the amount of the mass variation of the adsorbed gas component over time, as shown in Equation (2) [12]. Although the HSDM model is much closer to the real state, the complex solving process limits its practical applications.

$$\frac{dq}{dt} = 6q^* \sum_{n=1}^{\infty} \frac{D_c}{r_0^2} \exp \left[- (n\pi)^2 \frac{D_c}{r_0^2} t \right] \quad (2)$$

Second, the local equilibrium model is proposed for the strong-adsorbed component on the adsorbent material, which assumes that the mass transfer between solid adsorbent particles and external gas instantaneously completes, regardless of the mass transfer resistance. Thus, the second model only works for some ideal states, such as CO₂/N₂ separation on activated carbon.

Finally, a first-order linear-driving-force (LDF) model was proposed by Lagergren [39], which suggests that the uptake rate of a species into the adsorbent is proportional to the linear difference between the concentration of the species at the outer surface of the particle (equilibrium adsorption capacity) [40]. The average concentration within the particle is expressed as:

$$\frac{\partial q}{\partial t} = k_1(q_e - q) \quad (3)$$

where k is the rate constant (1/s), which can be approximated by $15D_e/r_c^2$, and D_e/r_c^2 is the diffusion-time constant. The LDF mass transfer coefficient plays a considerable role in the flow and adsorption process through a breakthrough experiment. Ma et al. [41] found that a lower LDF mass transfer reduced the appearance time of the breakthrough point but extended the completion time of the adsorption process. Moreover, the conventional LDF equation is verified to underestimate the adsorption rate in the initial stage. Li et al. [40] proposed an improved LDF equation derived from the parabolic concentration profile for

the intraparticle adsorbate, to eliminate the flaw of the conventional LDF concentration profile assumption, expressed as:

$$\frac{\partial q}{\partial t} = \frac{15D_e}{R^2} \left(q_e + 0.2789q_e e^{-\frac{q}{2q_e}} - q \right) \quad (4)$$

2.2. Pressure-Drop Model

A continuous PSA process is implemented through circulating changes in pressure. Thus, a pressure drop in the adsorption bed will directly affect the recovery and purity of the product. However, in a situation of low adsorption pressure or short cycle time, several computational studies indicate that the pressure drop has a limited effect on the overall process performance. Aaron [42] experimentally confirmed that the effect of a pressure drop was negligible on process performance in the flow regime; namely, the pressure drop concerns were not reasonable for small-scale air separation processes using similar column lengths (9.8–19.6 cm) and particle sizes (0.5 mm). When considering the energy consumption of the process, the pressure drop model is a key concern, since a higher pressure drop leads to a lower energy-storage efficiency [43]. The Darcy model assumes that the pressure drop is proportional to the flow rate, as expressed by Equation (5).

$$\nabla p = -\frac{\mu}{\alpha} v \quad (5)$$

where μ is the kinetic viscosity and α is the permeability, which is an important consideration in this model. Furthermore, the Ergun equation combines the description of pressure drops by the Carman–Kozeny equation for laminar flow and the Burke–Plummer for turbulent flow, which is more appropriate in packed adsorbing columns, as expressed by Equation (6) [44].

$$-\frac{\partial P}{\partial z} = \frac{150\mu_g(1-\varepsilon_b)^2 u}{\varepsilon_b^3 d_p^2} + \frac{1.75\rho_g(1-\varepsilon_b)u^2}{\varepsilon_b^2 d_p} \quad (6)$$

2.3. Fluid-Flow Model

Fluid-flow models in a fixed bed include plug flow, plug flow with axial dispersion, and 2-dimensional (2D) radial dispersion flow, while the last term can be ignored because the adsorption bed diameter is much larger than that of particles.

Currently, most PSA process numerical simulations are governed by 1-dimensional (1D) models, without radial variation in the gas concentration, temperature and pressure. As the development of available powerful computer resources raises, there is an interest in extending these 1D adsorption modeling approaches into 2D/3D configurations. Compared to the 1D model, the 2D/3D models seem to be more accurate in terms of heat- and mass-transfer results, as more flow directions are taken into consideration [45]. In addition, it is more intuitive to reflect the distribution of some parameters (mole fractions, temperature, pressure and so on) in the adsorption bed. Moreover, a 3D model can be used in complex bed geometries or perform research on the equipment in the column, such as gas distributor optimization [46]. However, with the increase in dimensions, the number of computations is increased, meaning that it should take a long time to run the required simulations.

2.4. Special Treatments for Energy Balance

2.4.1. Heat of Adsorbed Phases and the Heat of Adsorption

The heat of the adsorbed phases for each component is a function of the loading and the temperature in the solid phases, the adsorbed phase heat capacity, and the solid density, as shown in Equation (7). Wang et al. found that the adsorbed phase would influence the

effective thermal conductivity of an adsorption bed, but this effect could be ignored under certain temperature conditions [47].

$$H_i = \rho_s C_{pai} w_i \frac{\partial T_s}{\partial t} \quad (7)$$

The rate of heat generation by the adsorption of each component i per unit mass of solid, depends on the local rate of mass transfer:

$$HT_i = \frac{\partial w_i}{\partial t} \Delta H_i \quad (8)$$

These rates are held in vectors, HT , and summed for all components, to obtain the total rate of heat generation by adsorption per unit volume of solid:

$$\rho_s \sum_i (-HT_i) \quad (9)$$

2.4.2. Non-Isothermal Conditions and Thermal Equilibrium

For non-isothermal conditions, an additional heat transfer coefficient resistance between the adsorbent and gas introduces what can be calculated as follows:

$$\text{rate of heat transferred per m}^3 \text{ of bed} = HTC a_p (T_g - T_s) \quad (10)$$

When gas and solid are in thermal equilibrium, $T_g = T_s$.

2.4.3. Adiabatic, Thin-Wall, and Rigorous Models of Heat Transfer to Environment

Adiabatic condition means no heat transfer occurs between the bed and the wall. For thin wall, the heat exchange between the gas in the bed and the environment is included in the gas-phase energy balance as:

$$\frac{4H_w}{D_B} (T_g - T_{amb}) \quad (11)$$

A rigorous model includes a wall-energy-balance equation that contains the following terms: heat transfer from the gas in the bed to the inner wall; heat transfer from the outer wall to the environment (including the influence of any insulating material); axial thermal conduction along the wall; and heat accumulation within the wall material. The governing equation is:

$$-k_w \frac{\partial^2 T_w}{\partial z^2} + \rho_w c_{pw} \frac{\partial T_w}{\partial t} - H_w \frac{4D_B}{(D_B + W_T)^2 - D_B^2} (T_g - T_w) + H_{amb} \frac{4(D_B + W_T)^2}{(D_B + W_T)^2 - D_B^2} (T_w - T_{amb}) = 0 \quad (12)$$

Abd et al. studied the three heat transfer models mentioned above on CO₂ separation properties in a biomethane-upgrading system. The result showed that highest methane purity of 97% was presented in the rigorous model, followed by thin-wall (93%) and adiabatic (92%) systems. The rigorous model can help in the design of a new PSA system that can recuperate heat during the adsorption and desorption steps, for effective adsorption and regeneration.

2.5. One-Dimensional Process Model

Usually, there are five basic cycle steps associated with any PSA process: adsorption, pressure equalization, purge/rinse, co-current or counter-current depressurization (blow-down) and re-pressurization steps, which can be scheduled in many different ways for a typical PSA process with multiple beds [48]. Many previous works reported approaches for a complex PSA-cycle scheduling, involving a priori specification of the cycle steps, their sequence, and the number of beds, and then following a systematic procedure based

on a few simple rules, some heuristics, and some experience [49–51]. Switching between different operation steps is expressed numerically as a change in boundary conditions. The general boundary conditions for each step are listed in Table 1. Aspen Adsorption™ is an industrially acclaimed software for multistep coupled process design and assessing feasibility-model development and simulation [47]. Considering the current computing power constraints, most process designs based on Aspen Adsorption™ adopted a 1D mathematic model with an adsorption-bed model and auxiliary-module models, which are summarized in Tables 2 and 3, respectively [52–57]. However, the 1D model cannot describe the fine characteristics directly, such as the adsorber structure, adsorbent packed form and single particle internal morphology, nor their influence on the adsorption-mass transfer, resulting in the inability to accurately predict the local component concentration and other information in the adsorption process. More personalized programming software, such as gPROMS, as well as the computational-flow-dynamics method for the in-depth study of mass transfer between gas–solid phases, can be used to assist the process design.

Table 1. Boundary conditions for each step.




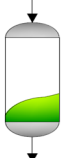

Step	Z = 0	Z = L
Adsorption 	$u_{0,\text{inlet}}C_{\text{inlet},i} \Big _{z=0} = u_0C_i - \varepsilon_b D_{ax} C \frac{\partial y_i}{\partial z}$ $u_{0,\text{inlet}}C_{\text{inlet}} \Big _{z=0} = u_0C$ $u_{0,\text{inlet}}C_{\text{inlet}}C_p T_{\text{inert}} \Big _{z=0} = u_0CC_p T_g - k_g \frac{\partial T_g}{\partial z}$	$P _{z=L} = P_{\text{outlet}}$ $\frac{\partial C_i}{\partial z} \Big _{z=L} = 0$ $\frac{\partial T_g}{\partial z} \Big _{z=L} = 0$
Equalization and co-current depressurization 	$\frac{\partial C_i}{\partial z} \Big _{z=0} = 0$ $u_0 _{z=0} = 0$ $\frac{\partial T_g}{\partial z} \Big _{z=0} = 0$	$\frac{\partial C_i}{\partial z} \Big _{z=L} = 0$ $P _{z=L} = P_{\text{outlet}}$ $\frac{\partial T_g}{\partial z} \Big _{z=L} = 0$
Blowdown 	$\frac{\partial C_i}{\partial z} \Big _{z=0} = 0$ $P _{z=0} = P_{\text{outlet}}$ $\frac{\partial T_g}{\partial z} \Big _{z=0} = 0$	$\frac{\partial C_i}{\partial z} \Big _{z=L} = 0$ $u_0 _{z=L} = 0$ $\frac{\partial T_g}{\partial z} \Big _{z=L} = 0$
Purge 	$\frac{\partial C_i}{\partial z} \Big _{z=0} = 0$ $P _{z=0} = P_{\text{outlet}}$ $\frac{\partial T_g}{\partial z} \Big _{z=0} = 0$	$u_{0,\text{inlet}}C_{\text{inlet},i} \Big _{z=L} = u_0C_i - \varepsilon_b D_{ax} C \frac{\partial y_i}{\partial z}$ $u_{0,\text{inlet}}C_{\text{inlet}} \Big _{z=L} = u_0C$ $u_{0,\text{inlet}}C_{\text{inlet}}C_p T_{\text{inert}} \Big _{z=L} = u_0CC_p T_g - k_g \frac{\partial T_g}{\partial z}$
Equalization pressurization and Pressurization 	$\frac{\partial C_i}{\partial z} \Big _{z=0} = 0$ $u_0 _{z=0} = 0$ $\frac{\partial T_g}{\partial z} \Big _{z=0} = 0$	$u_{0,\text{inlet}}C_{\text{inlet},i} \Big _{z=L} = u_0C_i - \varepsilon_b D_{ax} C \frac{\partial y_i}{\partial z}$ $u_{0,\text{inlet}}C_{\text{inlet}} \Big _{z=L} = u_0C$ $u_{0,\text{inlet}}C_{\text{inlet}}C_p T_{\text{inert}} \Big _{z=L} = u_0CC_p T_g - k_g \frac{\partial T_g}{\partial z}$

Table 2. Mathematical model of 1D non-isothermal adsorption bed.

Category	Equation
Component mass balance	$\frac{\partial C_i}{\partial t} + \frac{(1-\varepsilon)}{\varepsilon} \rho_s \frac{\partial w_i}{\partial t} - D_{ax} \frac{\partial^2 C_i}{\partial z^2} + \frac{\partial(uC_i)}{\partial z} = 0$
Total mass balance	$\frac{\partial C}{\partial t} + \frac{(1-\varepsilon)}{\varepsilon} \rho_s \sum_{i=1}^n \frac{\partial w_i}{\partial t} + \frac{\partial(uC)}{\partial z} = 0$
Gas and Solid phase	$(\varepsilon \rho_g c_g + (1-\varepsilon) \rho_s c_s) \frac{\partial T}{\partial t} - (1-\varepsilon) \rho_s \sum_{i=1}^n (-\Delta H_i) \frac{\partial q_i}{\partial t} - \lambda_{ex} \frac{\partial^2 T}{\partial z^2} + \rho_g c_g \frac{\partial(uT)}{\partial z} + \frac{2h_i}{r_{b,i}} (T - T_w) = 0$
Bed wall	$\rho_w c_p \frac{\partial T_x}{\partial t} - Hw \frac{4D_B}{(D_B+W_T)^2 - D_B^2} (T_\varepsilon - T_w) + H_{amb} \frac{4(D_B+W_T)^2}{(D_B+W_T)^2 - D_B^2} (T_w - T_{am}) = 0$
Momentum balance	$\frac{\partial P}{\partial z} = - \left(\frac{1.5 \times 10^{-3} (1-\varepsilon_i)^2}{(2r_p \psi)^2 \varepsilon_i^3} \mu v_g + 1.75 \times 10^{-5} M \rho_g \frac{(1-\varepsilon_i)}{2r_p \psi \varepsilon_i^3} v_g^2 \right)$
Mass transfer	$\frac{\partial w_i}{\partial t} = MTC_{si} (w_i^* - w_i)$
Langmuir isotherm	$w_i = \frac{IP_i e^{IP_{2i}/T_s} P_i}{1 + \sum_k (IP_{3k} e^{IP_{4k}/T_s} P_k)}$
Ideal gas equation	$Py_i = RTc_i$

Table 3. Model equation of compressor, buffer and valve.

Category	Equation
Vacuum pump and compressor	<p>if outlet. P > inlet. P, then $dW = \frac{\text{inlet.p inlet. } V}{\eta_p} \frac{\gamma}{\gamma-1} \left[\left(\frac{\text{outlet. P}}{\text{inlet. P}} \right)^{\frac{\gamma-1}{\gamma}} - 1 \right]$</p> <p>if outlet. P ≤ inlet. P, then $dW = 0$; $W_{\text{total}} = \int_0^{t_{\text{cycle}}} dW$, $\gamma = 1.3$, $\eta_p = 0.8$.</p>
Buffer tank	<p>Mass balance: $\frac{\partial ni}{\partial t} - \sum F_i y_i + \sum F_O y_O = 0$ Energy balance: $\frac{\partial T(\sum niC_{pi})}{\partial t} - \sum_{i=1}^N F_i T_i \sum y_k C_{pg,i} + \sum_{O=1}^N F_O T_O \sum y_k C_{pg,i} = 0$</p>
Valve	<p>Unidirection: if inlet. P > outlet. P, then $F = Cv(\text{inlet. P} - \text{outlet. P})$; if inlet. P ≤ outlet. P, then $F = 0$</p> <p>Bidirection: $F = Cv(\text{inlet. P} > \text{outlet. P})$</p>
Purity (%)	$\text{Purity}_{\text{target}} (\%) = \frac{\int_0^{t_{\text{cycle}}} F_{\text{product,target}} y_{\text{product,target}} dt}{\int_0^{t_{\text{cycle}}} F_{\text{product}} dt}$
Recovery (%)	$\text{Recovery}_{\text{target}} (\%) = \frac{\int_0^{t_{\text{cycle}}} F_{\text{product,target}} y_{\text{product,target}} dt}{\int_0^{t_{\text{cycle}}} F_{\text{feed,target}} y_{\text{feed,target}} dt}$
Energy consumption (MJ/kg)	$E = \frac{\int_0^{t_{\text{cycle}}} \frac{P_{\text{out}} V_{\text{in}}}{\eta_p} \frac{\gamma}{\gamma-1} \left[\left(\frac{P_{\text{out}}}{P_{\text{in}}} \right)^{(\gamma-1)/\gamma} - 1 \right] dt}{M_{\text{target}} \int_0^{t_{\text{cycle}}} F_{\text{out}} y_{\text{out, target}} dt}$

3. PSA Numerical Optimization and Control

3.1. Optimization Strategies

The pressure-swing-adsorption process includes design parameters and operating variables such as bed size, selection of adsorbents, timing settings, duration of each step, adsorption and desorption pressures, P/F ratios, etc. [58]. Finding the best design and operation variables is an effective way to improve the efficiency of PSA process. However, design parameters and operating variables are always highly coupled with purity, recovery rate, productivity, energy consumption and other performance indicators, making it difficult to determine its optimal conditions through empirical methods. In addition, as PSA optimization is a typical multi-objective optimization problem, several objective functions may conflict with each other; for example, purity and recovery vary in the opposite direction [34,59,60]. Due to the mutual influence and tradeoff between different objective functions, a multi-objective optimization problem has a series of optimal solutions

(called the Pareto optimal set) rather than an optimal solution [61,62]. The projection of the Pareto optimal set onto space is called the Pareto front, or the Pareto curve for dual-objective optimization. Some researchers only focus on a single performance indicator of the PSA process, or convert the multi-objective optimization problem into a single-objective optimization problem by constructing a specific function [21].

A typical PSA-process optimization strategy is presented in Figure 2. In general, the numerical optimization process of PSA includes two aspects: the process model and optimization algorithm. The former is the process of obtaining the process performance through the input design and operation, while the latter is to determine the optimization direction according to objectives and constraints. The process model can be divided into two main parts: the detailed model and surrogate model, each of them corresponds to different optimization strategies and algorithms.

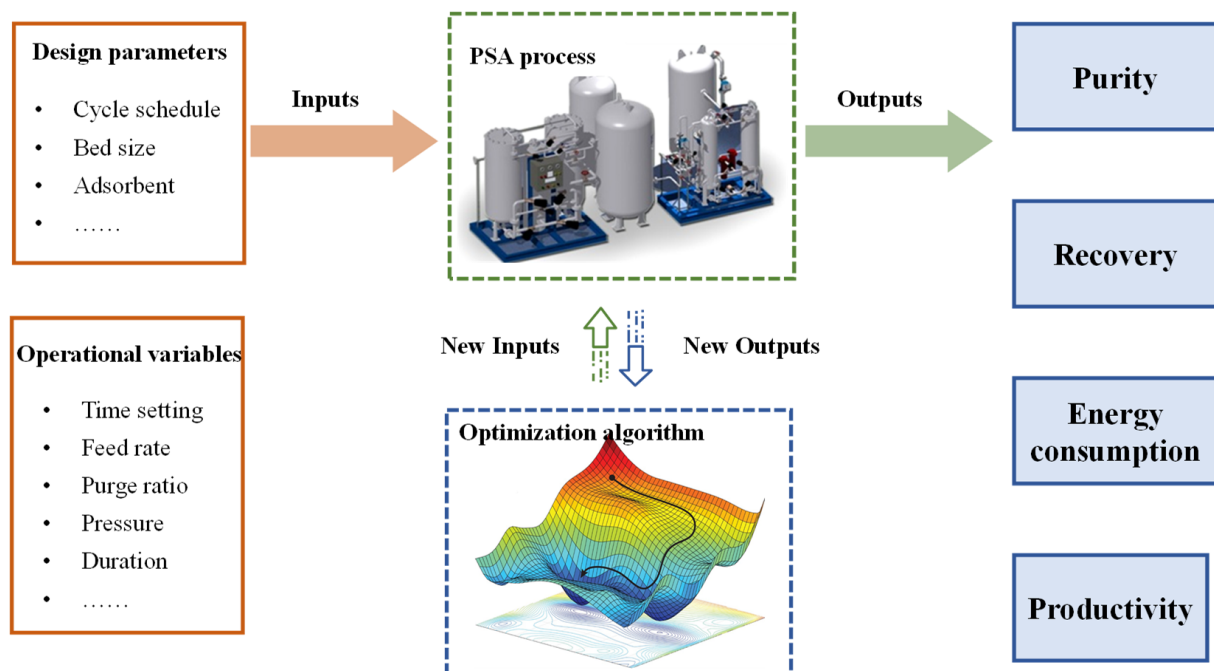


Figure 2. Typical PSA-process optimization strategies.

3.1.1. CSS Definition

It is worth mentioning that the numerically optimized results only make sense when achieving the cyclic steady state (CSS). However, the number of such cycles depends on the PSA set, operational sequence, and gas-adsorbent property, making it take a long time to be reached. Thus, a definition of an approximate CSS is employed, as shown in Equation (13) [63].

$$e_{css} = \max \left(\left| y_{t=N \cdot t_{cycle}} - y_{t=(N+1) \cdot t_{cycle}} \right| \right) \leq \epsilon_{css} \quad (13)$$

where y represents important PSA variables used for controlling the CSS, such as temperature, concentration, pressure, purity, and recovery; ϵ_{css} represents the solution accuracy of the definition of the cyclic steady state; and e_{css} is the absolute error of the definition of the cyclic steady state.

3.1.2. Detailed Model

The detailed model is formed by a series of partial differential and algebraic equations (PDAEs) and periodic boundary conditions. According to different methods, the detailed models mainly include single discretization (SD) and complete discretization (CD).

In the SD model approach, the PDAEs of the adsorption process is converted into differential algebraic equations (DAEs). This method only discretizes the space domain and uses the ode solver to solve in the time domain. The cyclic steady state of the PSA process is reached by switching the boundary conditions related to different steps in the cycle, which robustly processes simulation and optimization. The optimal decision value obtained by optimization is the same as the simulated process performance, and it is easier to initialize the convergence region than with the CD model.

In the CD model approach, the time domain and spatial domain are discretized simultaneously. The method directly couples the PDAEs system with the optimization problem, and the model equation is solved only once in the optimal state, avoiding too much computation work to obtain the intermediate solution and achieving a better numerical-computation ability and robustness. Nilchan et al. [64] first proposed the CD method by using the orthogonal configuration method to discretize the time domain, and the finite difference method to discretize the space domain. The computational costs of time integration were fully eliminated but this relied on the iteration of nonlinear algebraic equations. Calvin Tsay et al. [65] formulated a new set of pseudo-transient simulation and optimization principles for dynamic process models based on discretizing the temporal domain and spatial domain simultaneously.

In previous work, a nonlinear programming model such as the quadratic programming (QP) and sequential quadratic programming (SQP) algorithms are commonly used in for the PSA optimization based on the SD model. In order to solve large-scale nonlinear programming problems, which have a large number of equationally constrained equations but relatively low degrees of freedom, the reduced-space SQP (r-SQP) algorithm is proposed. The r-SQP can greatly reduce the amount of calculation and storage capacity of the optimization process through a spatial-decomposition technique that solves the process system in zero space, with relatively small degrees of freedom [31]. Currently, the algorithm has been successfully applied in nitrogen/methane separation, biogas upgrading, carbon capture, and other processes. Sun et al. [66] employed the state-of-the-art reduced space successive quadratic programming (r-SQP) optimization algorithm to find the optimal values of decision variables with additional constraints for N₂/CH₄ separation, which took nearly 64 h. Ding et al. [67] proposed a generic optimization framework, as shown in Figure 3. It contained the discretization and solution of the partial differential equations, the sensitivity of the decision variable, the judgment of CSS, and the choice of the optimization algorithm.

3.1.3. Surrogate Model

In order to simplify the computation of reaching CSS and reduce the computational consumption in the optimization process on the basis of the accuracy of the model, researchers proposed the surrogate model to replace the detailed model. The surrogate model generated from data-driven black-box functions, the central problem of which is learning to establish an input–output relationship that is as accurate and simple as possible from data obtained from simulations or experiments, instead of solving the equations. This model investigates the effect of operation parameters (valve, feed flow rate, adsorption time) on objective functions (purity, recovery, productivity, energy consumption) through a large number of experimental and simulation results.

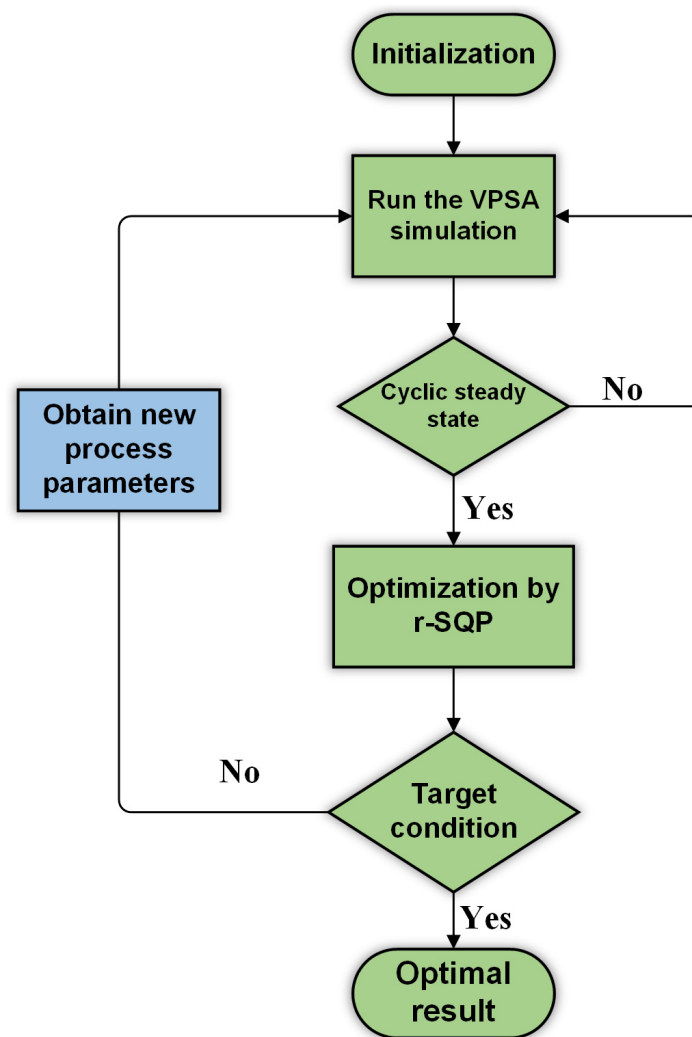


Figure 3. A generic optimization framework from Ding et al. [67]. Readapted with permission from Ref. [67]. Copyright 2018 Springer Nature.

The selection of a suitable and accurate model is critical for a PSA data-driven surrogate model. A deep-learning method along with an artificial neural network (ANN) can fully dig out the most essential laws of process data and quickly establish a surrogate model [28]. The backpropagation neural network (BP-NN) is frequently used, due to its excellent prediction and fitting capabilities. A typical multilayer feedforward neural network structure is shown in Figure 4. The basic training process is as follows: first, a number of decision variables and objective functions are selected, and then the training samples are obtained from the detailed PSA model. Then, the ANN toolbox in MATLAB is used to take the decision variables of samples as input and the objective function values calculated by the detailed model as output. Finally, the algorithm is allowed to train itself by adjusting the proportion of the training set, validation set and test set. If the fit obtained from the training does not meet the requirements, the percentages of the three sets are changed and retrained. Lee et al. [60] trained and tested a dynamic-model ANN for H₂ recovery and CO₂ capture from the tail gas of hydrogen plants, and they found that the dynamic-model-based ANN could precisely predict the dynamic behavior and optimum performance of an integrated process at a low computational cost.

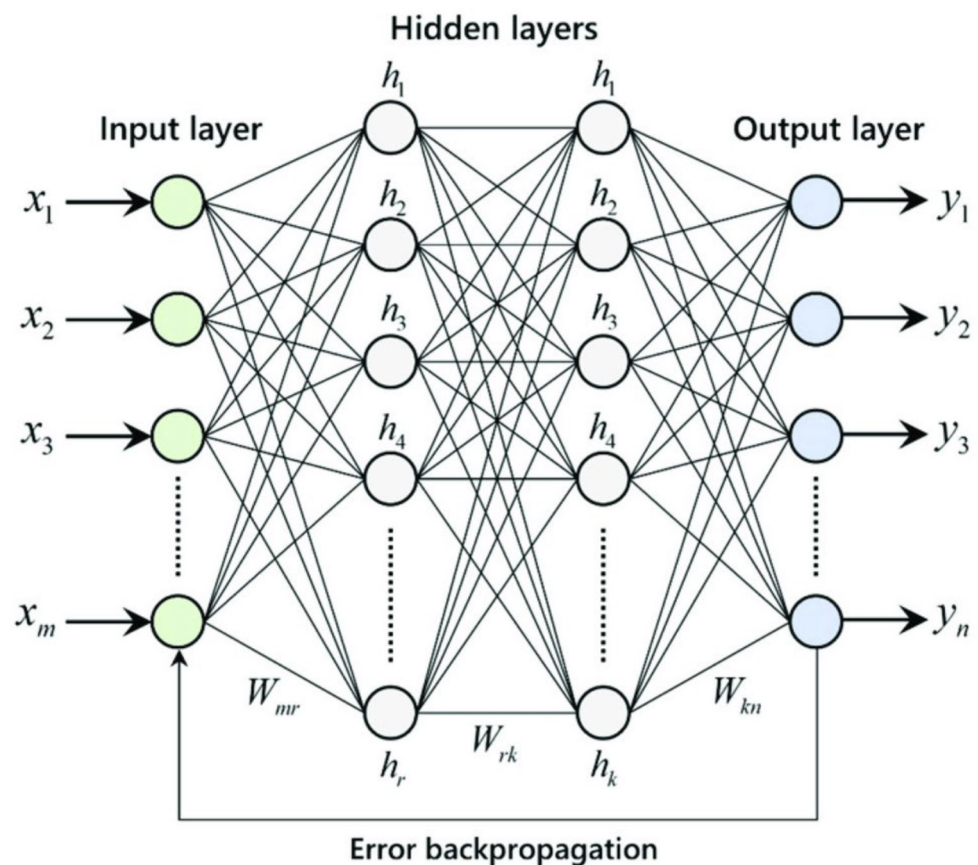


Figure 4. Schematic diagram of a multilayer feedforward network trained using the BP algorithm.

In addition to ANN, applications of other surrogate models, such as response surface models, Kriging models, polynomial models, orthogonal configuration models, support vector machines, and gaussian processes regression, have been reported as well. Karson [68] proposed and tested a model-reduction-based approach that systematically generates low-order representations of rigorous PSA models. M. Moustapha [69] performed a detailed comparative study of Kriging and support vector regression (SVR). Both models are considered with isotropic or anisotropic kernels, but the Kriging model had a higher accuracy than SVR and fewer failed cases. Considering real configurations instead of the experimental design, anisotropic L_2 -SVR with Matérn seemed to be consistently the best model. Alison Cozad and Nikolaos V. Sahinidis [70] designed a software package called automated learning of algebraic models for optimization (ALAMO) to automate the proposed methodology, which was able to identify accurate, low-complexity algebraic models that approximate a variety of high-fidelity systems. Zhang et al. [71] implemented the Box–Behnken design methodology (BBD), a type of response surface method, on the operating-parameter optimization of hydrogen purification. The flow chart of the BBD method is shown in Figure 5. They put the data from Aspen simulated results into Design Expert™ solved through the BBD method to obtain optimized operating conditions and then validated the predictions by comparison with the Aspen recalculated results. In the BBD method, desirability is an objective function that ranges from zero (outside of the limits of the performance objectives) to one (where the performance objectives are met). Shen et al. [72] applied the central composite design methodology to design experiments of the VPSA process, which explained the effects of the P/F ratio, adsorption time and desorption pressure on product purity, recovery and process energy consumption.

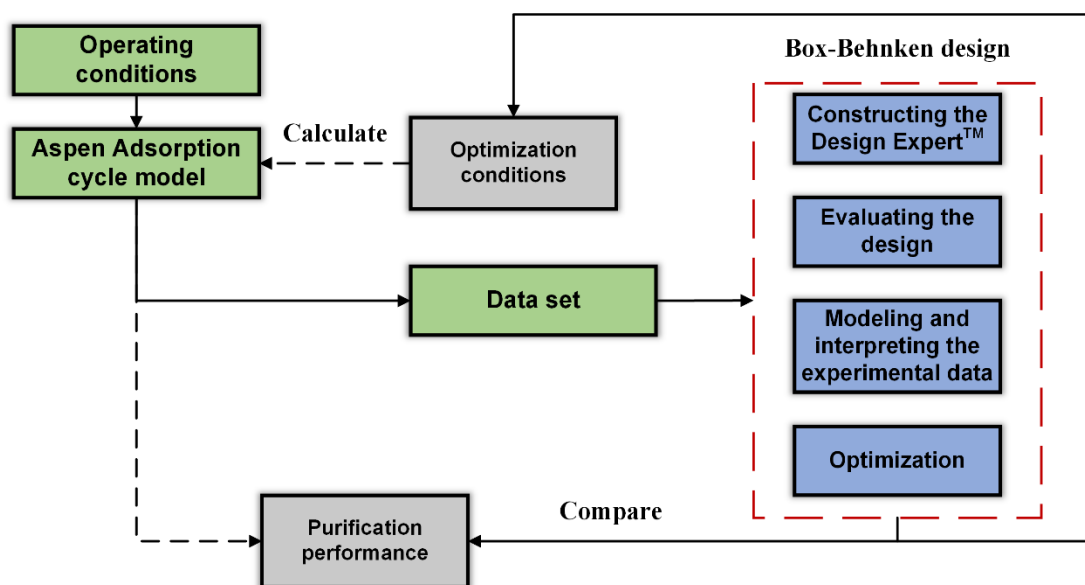


Figure 5. Flow chart of the BBD method for the PSA process cited by Zhang et al. [71]. Readapted with permission from Ref. [71]. Copyright 2021 Elsevier.

With the development of computer, mathematics and other disciplines and the progress of computing power, artificial-intelligence (AI) technology has made significant progress and breakthroughs in recent years, especially in the fields of image vision, automatic driving, scene prediction and robotics [73]. The industry 4.0 era combines physical and digital with advanced technologies such as big data, artificial intelligence, machine learning, etc., providing a new approach to the process industry that is more comprehensive, interconnected and smarter [33,74]. AI-based optimization algorithms are more widely used than traditional optimization algorithms. Several studies have used novel metaheuristic and AI-based optimization algorithms, including the genetic algorithm (GA) and particle swarm optimization (PSO) [75,76]. Perez [66] combined experiments with a genetic algorithm to obtain Pareto curves for the multi-objective optimization of the enrichment of CO₂ from a mixture of 15% CO₂ + 85% N₂. The performance indicators, such as CO₂ purity and recovery, the transients of temperatures, outlet flow and composition, showed an excellent match with the experiments. Compared with ordinary genetic algorithms, the second-generation nondominated sorting genetic algorithm (NSGA-II) (1) has excellent robustness to multi-objective optimization; (2) can avoid local minima caused by initial value guessing, and can provide the Pareto optimal solution set; (3) is capable of easily parallelizing processing on multi-core computing devices, greatly reducing the running time; (4) can be used to know the experimental design and process design; (5) can be combined with the ANN surrogate model, when it can meet optimization processes requiring a large number of computing samples without additional computing power consumption.

3.2. Control Strategy

In an actual PSA process, performance indicators will deviate from the set value or fail due to the performance degradation of the device, fluctuations in upstream and downstream processes, changes in external conditions, and the setting of process goals. Therefore, it is necessary to apply a real-time control to the PSA process and adjust the operating parameters to keep the process performance at the set state. At present, the control strategies used in the industry are mainly divided into proportional-integral-differential control (PID) and advanced process control (APC) [77,78]. PID is a control strategy that combines three control laws: proportional (P), integral (I) and differential (D). It determines the current control input based on the deviation of the current and past output measurements of the process from the set value. Xing et al. [16] used a PID method for controlling two cases: in case 1, the CO₂ concentration of the feed decreased from 15% to 12%, and in

case 2, it varied randomly from between 12% and 15%. The results reflected that the control with a PID closed-loop loop had a good correction effect on the process disturbance, in addition to a good control effect on the product gas concentration. Akulinin [79] developed an adaptive 2-level SCADA system with a PID controller for 4-adsorption PSA plants for hydrogen production with a purity of 96–99 vol.%, which could continuously control the current values of disturbing actions and maintain the current-optimum adsorption pressure. When the disturbing actions deviate from the nominal values at the upper level, a personal computer promptly solves the optimization problem, and then the automatic control system regulators obtain the current optimal tasks to recalculate valve operation by a programming regulator. However, for a highly complex system with interrelated variables such as the PSA process, the PID controller has great limitations. First, the PID controller can only control after the deviation action occurs, which often requires many steps to stabilize the controlled variable to the set value and leads to some fluctuations. Second, after changing the operating conditions, the PSA process needs a large stabilization time and long feedback delay. Third, the PID controller can only complete the control of single input–single output. For the increasingly complex PSA process, it cannot explain the highly coupled relationship between the controlled variables and the controlled inputs. Fourth, it is not suitable for controlling operating conditions with constraints. With the development of computing power, advanced process control has been applied to handle the above problems.

Advanced process control (APC) is a general term that is different from classical PID control methods. In a broad sense, any control strategy that can achieve better control effects than PID control can be called APC. In terms of the development sequence, APC can be roughly divided into three categories: one is the traditional advanced control technology, such as variable gain control, time-delay compensation control, decoupling control, selective control, etc.; the second is the current advanced control technology, such as model-predictive control (MPC), statistical-quality control (SQC), adaptive control, expert control, neural controller, fuzzy control, optimal control, robust predictive control, etc. At present, MPC is widely used and has achieved good results.

MPC takes many forms, such as model-algorithmic control (MAC), dynamic-matrix control (DMC), extended time-domain-adaptive control (EPSAC), generalized predictive control (GPC), and internal-mode control (IMC). Compared with the standard PID-based controller, MPC provides the optimal control plan based on the deviation between the current and past values, along with a predictive model to predict future deviations in order to determine the current optimal input strategy in a rolling optimization. All predictive algorithms have some common features: model prediction, rolling optimization, and feedback correction. Han et al. [80] realized the interactive calculation between gPROMS and MATLAB, and used MPC to correct disturbances. Jesse [81] designed and implemented two controllers (optimal MPC and fuzzy PD + I) into the PSA process of separating a water–ethanol mixture to maintain the desired purity, track a path and reject disturbances, as shown in Figure 6. According to their results, Optimal MPC required a lower number of cycles compared with the Fuzzy PD + I controller; however, it only kept the purity within the allowed ranges rather than tracking the trajectory desired. A novel artificial intelligence-oriented economic nonlinear model predictive control (EMPC) strategy was proposed by Márcio et al. The EMPC controller, combined with a deep-learning neural network (DNN), allows to obtain solutions at a low computational cost, making it more feasible in practice [35].

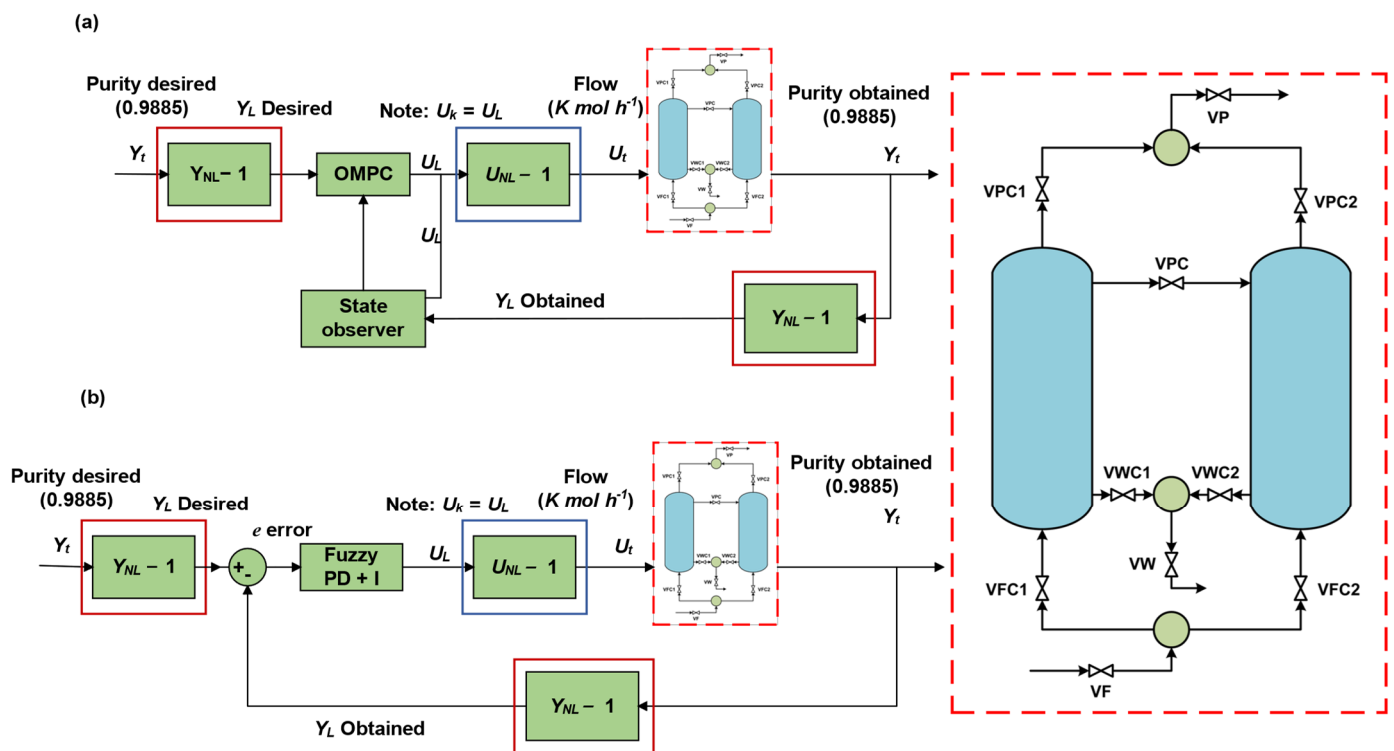


Figure 6. Simulation implementation within the Aspen Plus/Simulink environment of (a) the optimal MPC and (b) fuzzy PD + I to control the adsorption plant cited from Jesse [81]. U_L and Y_L are the input–output control signals, whereas U_t and Y_t are the input–output signals of PSA process. VP, VF and VW are product valve, feed valve and waste valve, respectively. Readapted with permission from Ref. [81]. Copyright 2020 Elsevier.

4. Conclusions and Future Work

In this article, we reviewed the numerical research on PSA-process modelling, optimization and control. A complete PSA-process model consists of a series of PDAEs, including the adsorption bed, auxiliary devices, boundary conditions and performance indicators. The optimization of PSA is based on the process model and optimization algorithm. The detailed model and surrogate model are two types of special treatment for the process model. The former solves the process model by discretizing in space or both in time and space simultaneously, while the latter is committed to establishing an input–output relationship that is as accurate and simple as possible from data obtained from simulations or experiments instead of solving the equations. As a surrogate model, ANN has excellent prediction and fitting capabilities, which can provide a large number of samples without additional computing-power consumption for the artificial-intelligence-based optimization algorithm. Process control is necessary when facing external disturbances or parameter fluctuations. The main reason for the MPC control being superior to PID control is owing to its prediction ability.

With the improvement in computer computing performance, more issues deserve to be noticed. First, the overlapping and cooperative efforts of adsorbent research and process development should be achieved. On the one hand, the ideal adsorbent used for target-gas adsorption should have a large working capacity, fast adsorption/desorption kinetics, low adsorption heat, and high selectivity. Moreover, adsorbent materials are required to be inexpensive, practically shaped, have stable thermal and mechanical properties, and be recyclable in the industrial process. Thus, a comprehensive adsorbent database containing well-organized, easily accessible data about available adsorbents can be of great value for researchers and engineers and serve as a useful basis for further adsorbent development efforts. On the other hand, the processes' engineering involves column

geometry, adsorbent-loading ratio, and time-step settings, which usually have a very deep impact on the performance of PSA process. In fact, it is a multiscale problem containing microscopic pore structure characteristics within particles, a mesoscale particle layer packed network, and macroscopic device structure. A complete computational mass-transfer model for adsorption remains to be established. Second, as PSA industrial applications scale up, problems such as large pressure drops, void volumes and uneven fluid distribution are extremely prominent. VPSA/PSA system operation is greatly affected by pressure drops and void volumes within the adsorbent bed. A bed-pressure drop is the main cause of inefficiency in the VPSA/PSA process, due to the large amount of throughput with high superficial velocity at sub-ambient/ambient pressures. The losses caused by a bed-pressure drop typically account for 10–15% of the total power consumption. The gas left in the void volume is meaninglessly pressurized or emptied, or even enriched in the product, which affects the quality of the subsequent purge section. An earlier local breakthrough caused by the heterogeneity of flow distribution along the axis also notably reduce the adsorbent efficiency. In the field of large-scale air separation, to solve these problems, a radial flow adsorber has been proposed as an alternative to the axial flow adsorber for CO₂/H₂O removal from the pretreatment layer. However, it also places higher demands on the adsorbent arrangement, gas distributor and inlet channel design. Last but not least, the current optimization or control models should be combined with the actual production process, because laboratory-scale experiments cannot provide a large amount of data, and only numerical simulation methods will inevitably lead to large deviations from the actual situation. Nevertheless, a set of actual facilities often runs for several decades, which means the real massive data accumulates continuously during this period. If deep-learning technology is applied to this, a more accurate alternative model will definitely be obtained, which, in turn, can guide the process design. In addition, the automation and intelligentization of PSA-process control may lead to potential risks, such as delayed or excessive regulation, which puts forward higher requirements for system stability and computing efficiency.

Author Contributions: Writing—original draft preparation, R.Z.; Writing—review and editing, Y.S., Z.T., W.L. and D.Z. All authors have read and agreed to the published version of the manuscript.

Funding: This research was funded by the National Key R & D Program of China, grant number: 2019YFB1505000.

Institutional Review Board Statement: Not applicable.

Informed Consent Statement: Not applicable.

Data Availability Statement: Not applicable.

Conflicts of Interest: The authors declare no conflict of interest.

References

1. Mehrotra, A.; Ebner, A.D.; Ritter, J.A. Arithmetic approach for complex PSA cycle scheduling. *Adsorption* **2010**, *16*, 113–126. [[CrossRef](#)]
2. Guan, Z.; Wang, Y.; Yu, X.; Shen, Y.; He, D.; Tang, Z.; Li, W.; Zhang, D. Simulation and analysis of dual-reflux pressure swing adsorption using silica gel for blue coal gas initial separation. *Int. J. Hydrogen Energy* **2021**, *46*, 683–696. [[CrossRef](#)]
3. Sees, M.D.; Kirkes, T.; Chen, C.-C. A simple and practical process modeling methodology for pressure swing adsorption. *Comput. Chem. Eng.* **2021**, *147*, 107235. [[CrossRef](#)]
4. Shi, W.; Yang, H.; Shen, Y.; Fu, Q.; Zhang, D.; Fu, B. Two-stage PSA/VSA to produce H₂ with CO₂ capture via steam methane reforming (SMR). *Int. J. Hydrogen Energy* **2018**, *43*, 19057–19074. [[CrossRef](#)]
5. Zhou, Y.; Shen, Y.; Fu, Q.; Zhang, D. CO enrichment from low-concentration syngas by a layered-bed VPSA process. *Ind. Eng. Chem. Res.* **2017**, *56*, 6741–6754. [[CrossRef](#)]
6. Shen, Y.; Zhou, Y.; Li, D.; Fu, Q.; Zhang, D.; Na, P. Dual-reflux pressure swing adsorption process for carbon dioxide capture from dry flue gas. *Int. J. Greenh. Gas Control* **2017**, *65*, 55–64. [[CrossRef](#)]
7. Feng, L.; Shen, Y.; Wu, T.; Liu, B.; Zhang, D.; Tang, Z. Adsorption equilibrium isotherms and thermodynamic analysis of CH₄, CO₂, CO, N₂ and H₂ on NaY Zeolite. *Adsorption* **2020**, *26*, 1101–1111. [[CrossRef](#)]

8. Rosner, F.; Chen, Q.; Rao, A.; Samuelsen, S.; Jayaraman, A.; Alptekin, G. Thermo-economic analyses of IGCC power plants employing warm gas CO₂ separation technology. *Energy* **2019**, *185*, 541–553. [[CrossRef](#)]
9. Marcoberardino, G.D.; Vitali, D.; Spinelli, F.; Binotti, M.; Manzolini, G. Green hydrogen production from raw biogas: A techno-economic investigation of conventional processes using pressure swing adsorption unit. *Processes* **2018**, *6*, 19. [[CrossRef](#)]
10. Grande, C.A. Advances in pressure swing adsorption for gas separation. *Int. Sch. Res. Not.* **2012**, *2012*, 982934. [[CrossRef](#)]
11. Ben-Mansour, R.; Habib, M.A.; Bamidele, O.E.; Basha, M.; Qasem, N.A.A.; Peedikakkal, A.; Laoui, T.; Ali, M. Carbon capture by physical adsorption: Materials, experimental investigations and numerical modeling and simulations—A review. *Appl. Energy* **2016**, *161*, 225–255. [[CrossRef](#)]
12. Li, S.; Deng, S.; Zhao, L.; Zhao, R.; Lin, M.; Du, Y.; Lian, Y. Mathematical modeling and numerical investigation of carbon capture by adsorption: Literature review and case study. *Appl. Energy* **2018**, *221*, 437–449. [[CrossRef](#)]
13. Xiao, Y.; Qiu, S.; Zhao, Q.; Zhu, Y.; Godiya, C.B.; He, G. Numerical simulation of low-concentration CO₂ adsorption on fixed bed using finite element analysis. *Chin. J. Chem. Eng.* **2020**, *36*, 47–56. [[CrossRef](#)]
14. Golubyatnikov, O.; Akulinin, E.; Dvoretzky, S.; Dvoretzky, D. To the problem of forming the equation system for pressure swing adsorption mathematical model. *Chem. Prod. Process Model.* **2021**. [[CrossRef](#)]
15. Li, D.; Zhou, Y.; Shen, Y.; Sun, W.; Fu, Q.; Yan, H.; Zhang, D. Experiment and simulation for separating CO₂/N₂ by dual-reflux pressure swing adsorption process. *Chem. Eng. J.* **2016**, *297*, 315–324. [[CrossRef](#)]
16. Xing, R.; Shi, W.; Shen, Y.; Liu, B.; Zhang, D. Vacuum pressure swing adsorption system for N₂/CO₂ separation in consideration of unstable feed concentration. *Adsorption* **2019**, *25*, 1147–1158. [[CrossRef](#)]
17. Fu, Q.; Yan, H.; Shen, Y.; Qin, Y.; Zhang, D.; Zhou, Y. Optimal design and control of pressure swing adsorption process for N₂/CH₄ separation. *J. Clean. Prod.* **2018**, *170*, 704–714. [[CrossRef](#)]
18. Xu, M.; Wu, H.-C.; Lin, Y.S.; Deng, S. Simulation and optimization of pressure swing adsorption process for high-temperature air separation by perovskite sorbents. *Chem. Eng. J.* **2018**, *354*, 62–74. [[CrossRef](#)]
19. Chen, Q.; Rosner, F.; Rao, A.; Samuelsen, S.; Jayaraman, A.; Alptekin, G. Simulation of elevated temperature solid sorbent CO₂ capture for pre-combustion applications using computational fluid dynamics. *Appl. Energy* **2019**, *237*, 314–325. [[CrossRef](#)]
20. Haghpanah, R.; Majumder, A.; Nilam, R.; Rajendran, A.; Farooq, S.; Karimi, I.A.; Amanullah, M. Multiobjective optimization of a four-step adsorption process for postcombustion CO₂ capture via finite volume simulation. *Ind. Eng. Chem. Res.* **2013**, *52*, 4249–4265. [[CrossRef](#)]
21. Anna, H.R.S.; Barreto, A.G., Jr.; Tavares, F.W.; de Souza, M.B., Jr. Machine learning model and optimization of a PSA unit for methane-nitrogen separation. *Comput. Chem. Eng.* **2017**, *104*, 377–391. [[CrossRef](#)]
22. Rashki, M.; Azarkish, H.; Rostamian, M.; Bahrpeyma, A. Classification correction of polynomial response surface methods for accurate reliability estimation. *Struct. Saf.* **2019**, *81*, 101869. [[CrossRef](#)]
23. Gaspar, B.; Teixeira, A.P.; Soares, C.G. Assessment of the efficiency of Kriging surrogate models for structural reliability analysis. *Probabilistic Eng. Mech.* **2014**, *37*, 24–34. [[CrossRef](#)]
24. Zheng, X.G.; Yao, H.; Huang, Y. Orthogonal numerical simulation on multi-factor design for rapid pressure swing adsorption. *Adsorption* **2017**, *23*, 685–697. [[CrossRef](#)]
25. Beck, J.; Friedrich, D.; Brandani, S.; Fraga, E.S. Multi-objective optimisation using surrogate models for the design of VPSA systems. *Comput. Chem. Eng.* **2015**, *82*, 318–329. [[CrossRef](#)]
26. Towne, A.; Schmidt, O.T.; Colonius, T. Spectral proper orthogonal decomposition and its relationship to dynamic mode decomposition and resolvent analysis. *J. Fluid Mech.* **2018**, *847*, 821–867. [[CrossRef](#)]
27. Zhang, D.; Lin, J.; Peng, Q.; Wang, D.; Yang, T.; Sorooshian, S.; Liu, X.; Zhuang, J. Modeling and simulating of reservoir operation using the artificial neural network, support vector regression, deep learning algorithm. *J. Hydrol.* **2018**, *565*, 720–736. [[CrossRef](#)]
28. Ye, F.; Ma, S.; Tong, L.; Xiao, J.; Bénard, P.; Chahine, R. Artificial neural network based optimization for hydrogen purification performance of pressure swing adsorption. *Int. J. Hydrogen Energy* **2019**, *44*, 5334–5344. [[CrossRef](#)]
29. Yu, X.; Shen, Y.; Guan, Z.; Zhang, D.; Tang, Z.; Li, W. Multi-objective optimization of ANN-based PSA model for hydrogen purification from steam-methane reforming gas. *Int. J. Hydrogen Energy* **2021**, *46*, 11740–11755. [[CrossRef](#)]
30. Xiao, J.; Li, C.; Fang, L.; Böwer, P.; Wark, M.; Bénard, P.; Chahine, R. Machine learning—Based optimization for hydrogen purification performance of layered bed pressure swing adsorption. *Int. J. Energy Res.* **2020**, *44*, 4475–4492. [[CrossRef](#)]
31. Xiao, J.; Mei, A.; Tao, W.; Ma, S.; Bénard, P.; Chahine, R. Hydrogen Purification Performance Optimization of Vacuum Pressure Swing Adsorption on Different Activated Carbons. *Energies* **2021**, *14*, 2450. [[CrossRef](#)]
32. Akulinin, E.; Golubyatnikov, O.; Dvoretzky, D.; Dvoretzky, S. Optimization and analysis of pressure swing adsorption process for oxygen production from air under uncertainty. *Chem. Ind. Chem. Eng. Q.* **2020**, *26*, 89–104. [[CrossRef](#)]
33. Nogueira, I.B.R.; Martins, M.A.F.; Regufe, M.J.; Rodrigues, A.E.; Loureiro, J.M.; Ribeiro, A.M. Big data-based optimization of a pressure swing adsorption unit for syngas purification: On mapping uncertainties from a metaheuristic technique. *Ind. Eng. Chem. Res.* **2020**, *59*, 14037–14047. [[CrossRef](#)]
34. Hao, Z.; Caspari, A.; Schweidtmann, A.M.; Vaupel, Y.; Lapkin, A.A.; Mhamdi, A. Efficient hybrid multiobjective optimization of pressure swing adsorption. *Chem. Eng. J.* **2021**, *423*, 130248. [[CrossRef](#)]
35. Martins, M.A.F.; Rodrigues, A.E.; Loureiro, J.M.; Ribeiro, A.M.; Nogueira, I.B.R. Artificial Intelligence-oriented economic non-linear model predictive control applied to a pressure swing adsorption unit: Syngas purification as a case study. *Sep. Purif. Technol.* **2021**, *276*, 119333. [[CrossRef](#)]

36. Zhou, L.; Qu, Z.G.; Chen, L.; Tao, W.Q. Lattice Boltzmann simulation of gas-solid adsorption processes at pore scale level. *J. Comput. Phys.* **2015**, *300*, 800–813. [[CrossRef](#)]
37. Weber, T.W.; Chakravorty, R.K. Pore and solid diffusion models for fixed-bed adsorbers. *AIChE J.* **1974**, *20*, 228–238. [[CrossRef](#)]
38. Inglezakis, V.J.; Fyrrillas, M.M.; Park, J. Variable diffusivity homogeneous surface diffusion model and analysis of merits and fallacies of simplified adsorption kinetics equations. *J. Hazard. Mater.* **2019**, *367*, 224–245. [[CrossRef](#)]
39. Haerifar, M.; Azizian, S. An exponential kinetic model for adsorption at solid/solution interface. *Chem. Eng. J.* **2013**, *215*, 65–71. [[CrossRef](#)]
40. Li, Z.; Liu, Y.; Wang, H.; Tsai, C.-J.; Yang, X.; Xing, Y.; Zhang, C.; Xiao, P.; Webley, P.A. A numerical modelling study of SO₂ adsorption on activated carbons with new rate equations. *Chem. Eng. J.* **2018**, *353*, 858–866. [[CrossRef](#)]
41. Ma, Q.; Chen, Z.; Liu, H. Multiple-relaxation-time lattice Boltzmann simulation for flow, mass transfer, and adsorption in porous media. *Phys. Rev. E* **2017**, *96*, 13313. [[CrossRef](#)] [[PubMed](#)]
42. Moran, A.; Talu, O. Role of pressure drop on rapid pressure swing adsorption performance. *Ind. Eng. Chem. Res.* **2017**, *56*, 5715–5723. [[CrossRef](#)]
43. Baghapour, B.; Rouhani, M.; Sharafian, A.; Kalhori, S.B.; Bahrami, M. A pressure drop study for packed bed adsorption thermal energy storage. *Appl. Therm. Eng.* **2018**, *138*, 731–739. [[CrossRef](#)]
44. Myers, T.G.; Font, F.; Hennessy, M.G. Mathematical modelling of carbon capture in a packed column by adsorption. *Appl. Energy* **2020**, *278*, 115565. [[CrossRef](#)]
45. Qasem, N.A.A.; Ben-Mansour, R. Adsorption breakthrough and cycling stability of carbon dioxide separation from CO₂/N₂/H₂O mixture under ambient conditions using 13X and Mg-MOF-74. *Appl. Energy* **2018**, *230*, 1093–1107. [[CrossRef](#)]
46. Qasem, N.A.A.; Ben-Mansour, R. Energy and productivity efficient vacuum pressure swing adsorption process to separate CO₂ from CO₂/N₂ mixture using Mg-MOF-74: A CFD simulation. *Appl. Energy* **2018**, *209*, 190–202. [[CrossRef](#)]
47. Ali Abd, A.; Roslee Othman, M.; Helwani, Z. Evaluation of thermal effects on carbon dioxide breakthrough curve for biogas upgrading using pressure swing adsorption. *Energy Convers. Manag.* **2021**, *247*, 114752. [[CrossRef](#)]
48. Ebner, A.D.; Mehrotra, A.; Ritter, J.A. Graphical approach for complex PSA cycle scheduling. *Adsorption* **2009**, *15*, 406–421. [[CrossRef](#)]
49. Ebner, A.D.; Mehrotra, A.; Ritter, J.A. Graphical unit block approach for complex PSA cycle scheduling of parallel interacting trains of columns and tanks. *Adsorption* **2015**, *21*, 229–241. [[CrossRef](#)]
50. Mehrotra, A.; Ebner, A.D.; Ritter, J.A. Simplified graphical approach for complex PSA cycle scheduling. *Adsorption* **2011**, *17*, 337–345. [[CrossRef](#)]
51. Ebner, A.D.; Ho, J.G.S.; Ritter, J.A. Graphical approach for formulating pressure swing adsorption cycle schedules with unlimited equalization steps. *Adsorption* **2018**, *24*, 221–232. [[CrossRef](#)]
52. Park, Y.; Kang, J.H.; Moon, D.K.; Jo, Y.S.; Lee, C.H. Parallel and series multi-bed pressure swing adsorption processes for H₂ recovery from a lean hydrogen mixture. *Chem. Eng. J.* **2021**, *408*, 127299. [[CrossRef](#)]
53. Liu, B.; Yu, X.; Shi, W.; Shen, Y.; Zhang, D.; Tang, Z. Two-stage VSA/PSA for capturing carbon dioxide (CO₂) and producing hydrogen (H₂) from steam-methane reforming gas. *Int. J. Hydrogen Energy* **2020**, *45*, 24870–24882. [[CrossRef](#)]
54. Lu, B.; Shen, Y.; Tang, Z.; Zhang, D.; Chen, G. Vacuum pressure swing adsorption process for coalbed methane enrichment. *Chin. J. Chem. Eng.* **2021**, *32*, 264–280. [[CrossRef](#)]
55. Golmakani, A.; Nabavi, S.A.; Manović, V. Production of negative-emission biomethane by twin double-bed pressure swing adsorption with tail gas sequestration. *Chem. Eng. J.* **2021**, *408*, 127312. [[CrossRef](#)]
56. Chen, Y.-F.; Lin, P.-W.; Chen, W.-H.; Yen, F.-Y.; Yang, H.-S.; Chou, C.-T. Biogas Upgrading by Pressure Swing Adsorption with Design of Experiments. *Processes* **2021**, *9*, 1325. [[CrossRef](#)]
57. Van Chinh, P.; Hieu, N.T.; Tien, V.D.; Nguyen, T.-Y.; Nguyen, H.N.; Anh, N.T.; Thom, D. Van Simulation and Experimental Study of a Single Fixed-Bed Model of Nitrogen Gas Generator Working by Pressure Swing Adsorption. *Processes* **2019**, *7*, 654. [[CrossRef](#)]
58. Durán, I.; Rubiera, F.; Pevida, C. Modeling a biogas upgrading PSA unit with a sustainable activated carbon derived from pine sawdust. Sensitivity analysis on the adsorption of CO₂ and CH₄ mixtures. *Chem. Eng. J.* **2022**, *428*, 132564. [[CrossRef](#)]
59. Subraveti, S.G.; Li, Z.; Prasad, V.; Rajendran, A. Machine learning-based multiobjective optimization of pressure swing adsorption. *Ind. Eng. Chem. Res.* **2019**, *58*, 20412–20422. [[CrossRef](#)]
60. Rebello, C.M.; Martins, M.A.F.; Rodrigues, A.E.; Loureiro, J.M.; Ribeiro, A.M.; Nogueira, I.B.R. A novel standpoint of Pressure Swing Adsorption processes multi-objective optimization: An approach based on feasible operation region mapping. *Chem. Eng. Res. Des.* **2022**, *178*, 590–601. [[CrossRef](#)]
61. Capra, F.; Gazzani, M.; Joss, L.; Mazzotti, M.; Martelli, E. MO-MCS, a derivative-free algorithm for the multiobjective optimization of adsorption processes. *Ind. Eng. Chem. Res.* **2018**, *57*, 9977–9993. [[CrossRef](#)]
62. Yang, L.; Zhu, A.; Shao, J.; Chi, T. A knowledge-informed and pareto-based artificial bee colony optimization algorithm for multi-objective land-use allocation. *ISPRS Int. J. Geo-Inf.* **2018**, *7*, 63. [[CrossRef](#)]
63. Khajuria, H.; Pistikopoulos, E.N. Optimization and control of pressure swing adsorption processes under uncertainty. *AIChE J.* **2013**, *59*, 120–131. [[CrossRef](#)]
64. Nilchan, S.; Pantelides, C.C. On the optimisation of periodic adsorption processes. *Adsorption* **1998**, *4*, 113–147. [[CrossRef](#)]
65. Tsay, C.; Pattison, R.C.; Baldea, M. A pseudo-transient optimization framework for periodic processes: Pressure swing adsorption and simulated moving bed chromatography. *AIChE J.* **2018**, *64*, 2982–2996. [[CrossRef](#)]

66. Sun, W.; Shen, Y.; Zhang, D.; Yang, H.; Ma, H. A systematic simulation and proposed optimization of the pressure swing adsorption process for N₂/CH₄ separation under external disturbances. *Ind. Eng. Chem. Res.* **2015**, *54*, 7489–7501. [[CrossRef](#)]
67. Ding, Z.; Han, Z.; Fu, Q.; Shen, Y.; Tian, C.; Zhang, D. Optimization and analysis of the VPSA process for industrial-scale oxygen production. *Adsorption* **2018**, *24*, 499–516. [[CrossRef](#)]
68. Leperi, K.T.; Yancy-Caballero, D.; Snurr, R.Q.; You, F. 110th Anniversary: Surrogate Models Based on Artificial Neural Networks To Simulate and Optimize Pressure Swing Adsorption Cycles for CO₂ Capture. *Ind. Eng. Chem. Res.* **2019**, *58*, 18241–18252. [[CrossRef](#)]
69. Moustapha, M.; Bourinet, J.-M.; Guillaume, B.; Sudret, B. Comparative study of Kriging and support vector regression for structural engineering applications. *ASCE-ASME J. Risk Uncertain. Eng. Syst. Part A Civ. Eng.* **2018**, *4*, 4018005. [[CrossRef](#)]
70. Cozad, A.; Sahinidis, N.V.; Miller, D.C. Learning surrogate models for simulation-based optimization. *AIChE J.* **2014**, *60*, 2211–2227. [[CrossRef](#)]
71. Zhang, N.; Bénard, P.; Chahine, R.; Yang, T.; Xiao, J. Optimization of pressure swing adsorption for hydrogen purification based on Box-Behnken design method. *Int. J. Hydrogen Energy* **2021**, *46*, 5403–5417. [[CrossRef](#)]
72. Shen, Y.; Shi, W.; Zhang, D.; Na, P.; Fu, B. The removal and capture of CO₂ from biogas by vacuum pressure swing process using silica gel. *J. CO₂ Util.* **2018**, *27*, 259–271. [[CrossRef](#)]
73. Dwivedi, Y.K.; Hughes, L.; Ismagilova, E.; Aarts, G.; Coombs, C.; Crick, T.; Duan, Y.; Dwivedi, R.; Edwards, J.; Eirug, A.; et al. Artificial Intelligence (AI): Multidisciplinary perspectives on emerging challenges, opportunities, and agenda for research, practice and policy. *Int. J. Inf. Manag.* **2021**, *57*, 101994. [[CrossRef](#)]
74. Zhong, R.Y.; Xu, X.; Klotz, E.; Newman, S.T. Intelligent manufacturing in the context of industry 4.0: A review. *Engineering* **2017**, *3*, 616–630. [[CrossRef](#)]
75. Gholami, A.; Bonakdari, H.; Ebtehaj, I.; Mohammadian, M.; Gharabaghi, B.; Khodashenas, S.R. Uncertainty analysis of intelligent model of hybrid genetic algorithm and particle swarm optimization with ANFIS to predict threshold bank profile shape based on digital laser approach sensing. *Measurement* **2018**, *121*, 294–303. [[CrossRef](#)]
76. Luan, J.; Yao, Z.; Zhao, F.; Song, X. A novel method to solve supplier selection problem: Hybrid algorithm of genetic algorithm and ant colony optimization. *Math. Comput. Simul.* **2019**, *156*, 294–309. [[CrossRef](#)]
77. Urich, M.D.; Vemula, R.R.; Kothare, M. V Multivariable model predictive control of a novel rapid pressure swing adsorption system. *AIChE J.* **2018**, *64*, 1234–1245. [[CrossRef](#)]
78. Hui, P.; Ping, W.; Weihua, L. Model Based Fractional Order PID Controller Design and Simulation of Pressure Swing Adsorption. In Proceedings of the 2019 Chinese Control Conference (CCC), Guangzhou, China, 27–30 July 2019; pp. 2880–2883.
79. Akulinin, E.I.; Ishin, A.A.; Skvortsov, S.A.; Dvoretzky, D.S.; Dvoretzky, S.I. Optimization of adsorption processes with cyclic variable pressure in gas mixture separation. *Adv. Mater. Technol.* **2017**, *3*, 51–60. [[CrossRef](#)]
80. Han, Z.-Y.; Xing, R.; Zhang, D.-H.; Shen, Y.-H.; Fu, Q.; Ding, Z.-Y.; Tian, C.-X. Vacuum pressure swing adsorption system for N₂/CH₄ separation under uncertainty. *Chem. Eng. Res. Des.* **2019**, *142*, 245–256. [[CrossRef](#)]
81. Rumbo Morales, J.Y.; López López, G.; Alvarado Martínez, V.M.; de J. Sorcia Vázquez, F.; Brizuela Mendoza, J.A.; Martínez García, M. Parametric study and control of a pressure swing adsorption process to separate the water-ethanol mixture under disturbances. *Sep. Purif. Technol.* **2020**, *236*, 116214. [[CrossRef](#)]